Citation for published item:

Frith, N. and Hilton, R.G. and Howarth, J.D. and Gröcke, D.R. and Fitzsimons, S.J. and Croissant, T. and Wang, J. and McClymont, E.L. and Dahl, J. and Densmore, A.L. (2018) 'Carbon export from mountain forests enhanced by earthquake-triggered landslides over millennia.', Nature geoscience., 11 (10). pp. 772-776.

Further information on publisher's website:

https://doi.org/10.1038/s41561-018-0216-3

Carbon export from mountain forests enhanced by earthquake-triggered landslides over millennia

Nicole V. Frith[1], Robert G. Hilton[1*], Jamie D. Howarth[2,3], Darren R. Gröcke[4], Sean J. Fitzsimons[5], Thomas Croissant[1], Jin Wang[1,6], Erin L. McClymont[1], Jenny Dahl[7], Alexander L. Densmore[1,6]

[1]Department of Geography, Durham University, Durham, DH1 3LE, UK

[2]GNS Science, Lower Hutt, New Zealand

[3]University of Victoria, Wellington, New Zealand

[4]Department of Earth Sciences, Durham University, Durham, DH1 3LE, UK.

[5]University of Otago, Dunedin, New Zealand

[6]Institute of Hazard, Risk and Resilience, Durham University, Durham, DH1 3LE, UK

[7]Rafter Radiocarbon Laboratory GNS Science, Lower Hutt, New Zealand.

*Correspondence to R.G.H. – r.g.hilton@durham.ac.uk, 0044 191 33 41970

Abstract

Rapid ground accelerations during earthquakes can trigger landslides which disturb mountain forests and harvest carbon from soils and vegetation. While infrequent over human timescales, these co-seismic landslides can set the rates of geomorphic processes over centuries to millennia. However, the long-term impacts of earthquakes and landslides on carbon export from the biosphere remain poorly constrained. Here, we examine the sedimentary fill of Lake Paringa, New Zealand, which is fed by a river draining steep mountains proximal to the Alpine Fault. Carbon isotopes reveal enhanced accumulation rates of biospheric carbon after four large earthquakes over the last ~1100 years, likely reflecting delivery of soil-derived carbon eroded by deep-seated landslides. Cumulatively these pulses of earthquake-mobilized carbon represent 23 ± 5% of the record length, but account for 43 ± 5% of the biospheric carbon in the core. Landslide simulations suggest that 14 ± 5 Mt C could be eroded in each earthquake. Our findings support a link between active tectonics and the surface carbon cycle and suggest that large earthquakes can significantly contribute to carbon export from mountain forests over millennia.

Main text

Earthquakes cause immediate damage to mountain forests[1,2], largely through earthquake-triggered landslides[2,3] which can completely strip hillsides of vegetation and soil[4]. Earthquakes have thus been viewed as a potential source of carbon dioxide (CO_2) over the years that follow, due to the direct forest damage and subsequent degradation of organic matter[1,2,5]. However, in steep mountain catchments, landslide debris can be transported rapidly to rivers[6] and buried within lake, delta, or marine deposits[7,8,9]. Active mountain belts are therefore thought to play an important role in setting the global discharge of biospheric organic carbon derived from vegetation and soil ($OC_{biosphere}$) by rivers of ~$0.16^{+0.07}_{-0.05}$ PgC yr^{-1} (refs. 10-11) and promote efficient OC burial due to high sediment loads, thereby contributing to sequestration of CO_2 over geological timescales[8,10,12]. It has proved difficult to quantify the long-term role of earthquakes in $OC_{biosphere}$ export because they are unpredictable, infrequent and sediment export after large earthquakes occurs over decades or longer[13,14]. If large earthquakes are not accounted for then short-term measurements of $OC_{biosphere}$ export by rivers[10,11] may be underestimated and fail to capture large transient changes in carbon fluxes over decadal time scales.

The immediate impacts of earthquake-triggered landslides have been observed in the sediment loads of numerous rivers[13-15]. Comparison with longer-term denudation rates show that earthquake-triggered landslides can account for a significant part of total denudation over 10^2-10^6 years[16-18]. In contrast, the only quantitative study of $OC_{biosphere}$ fluxes comes from the 2008 Wenchuan earthquake[19], mainly due to the need for river samples before and after the event. There,

$OC_{biosphere}$ discharge by the Sanping River doubled in the four years after the earthquake[19], but the brevity of the historical record meant that the roles of multiple earthquakes in driving $OC_{biosphere}$ export and CO_2 sequestration over longer time scales could not be determined. We address this using the sedimentary archive in Lake Paringa (Fig. 1), western Southern Alps, New Zealand[20]. The tectonic and geomorphic setting[21-23], climate[24] and extensive vegetation cover[25] make this an ideal location to quantify the impact of repeated earthquakes on biogeochemical cycles.

A lake record of earthquake-driven carbon transfers

The Alpine Fault extends almost continuously for > 650 km along the South Island of New Zealand and marks the transpressional boundary between the Australian and Pacific plates, with a shortening rate[23] of up to 12 mm yr^{-1}. No direct observations of Alpine Fault ruptures exist[26], but palaeoseismic reconstructions suggest that the fault ruptures along much of its length every 250-350 years[27-31], producing $M_w > 7.6$ earthquakes in A.D. 1717, ca. A.D. 1400, ca. A.D. 1150 and ~ca. A.D. 925[20,26]. Here we use a 6 m sediment core from the Windbag Basin of Lake Paringa which preserves evidence of these four Alpine Fault seismic cycles (Methods).

For each earthquake, three distinct sedimentary units have been identified[20]: i) co-seismic megaturbidites; ii) post-seismic hyperpycnites; and iii) inter-seismic layered silts. The co-seismic megaturbidites were deposited contemporaneously with fault rupture following sub-aqueous slope failures. Correlation of megaturbidites across multiple lakes[29,30] and their coincidence with earthquakes dated by other palaeoseismic methods[26-28] help to confirm them as markers of large earthquakes. These are overlain by post-seismic hyperpycnite stacks which contain sequences of graded turbidites[20]. These hyperpycnite stacks are central to this study: they record the landscape response to earthquake shaking and landslides in catchments draining to the lake. The overlying layered silts are interpreted as deposits from inter-seismic periods of relative geomorphic quiescence[20,29]. To quantify the accumulation of OC and assess the OC source[11], we combine measurements of total organic carbon (TOC) content ([TOC], wt.%), TOC to nitrogen ratio (C/N), stable organic carbon isotopes ($\delta^{13}C$), radiocarbon (^{14}C) activity in bulk organic matter reported as 'fraction modern' (F_{mod}), and biomarker abundance (Methods).

The upper part of the core (0.30–0.89 m) comprises the most recent sediments (from ~A.D. 1800 to ~ A.D. 1950) which characterize the OC accumulated during the present inter-seismic phase[20]. These sediments have mean $\delta^{13}C$ = –28.8 ± 0.2‰ (n = 19, ± 2SE unless otherwise stated) and mean C/N = 11.7 ± 0.5 (n = 19) (Supplementary Table S1). Organic matter from other inter-seismic silts in the core[20] has similar compositions (Fig. 2). The $\delta^{13}C$ and C/N values suggest that the inter-seismic sediments contain OC eroded from lower-elevation surface soils proximal to the lake (mean $\delta^{13}C$ = –29.9 ± 0.4‰ and C/N = 10.2 ± 2.0, n = 3; Supplementary Table S2), mixed with a contribution from surface and deep higher elevation soils (Fig. 3A). The role of autochthonous OC within the lake appears to be minor based on the distribution of n-alkanes and n-alkanoic acids (Supplementary Information, Supplementary Fig. 1). OC is also present in meta-sedimentary bedrock within the catchment, which tends to dominate the river bed sediment OC[32-34]. Bedrock samples have a mean [TOC] ~ 0.15 % (ref. 32), much lower than [TOC] in the inter-seismic sediments of 2.4 ± 0.3 %, (n = 50). We calculate that rock-derived OC makes up a minor component (~10%) of the inter-seismic sediments (Methods), similar to estimates from a small number of suspended sediment samples collected from the modern-day Hokitika and Whataroa Rivers[32].

Geochemical evidence for earthquake-triggered landslides

The post-seismic sediments deposited after each earthquake are ^{13}C-enriched, with a mean $\delta^{13}C$ = –27.2 ± 0.1‰, and have higher C/N values of 18.7 ± 1.4 (n = 97) compared to the inter-seismic layers (Figs. 2 and 3). The weighted mean post-seismic [TOC] = 2.2 ± 0.4 % (n = 97) is similar to the inter-seismic periods and rock-derived OC contributes a similar component (~10%). A rock-derived contribution therefore cannot explain the large shift in $\delta^{13}C$ and C/N values. The $\delta^{13}C$ and C/N values suggest that immediately following each earthquake, the OC is a mixture of ^{13}C-

enriched deeper soil (from deeper saprolite soil horizons[35] and weathered colluvium[34]) and surface soil from higher elevations (Fig. 3A).

Our inference of post-earthquake mobilisation of OC from deeper soil sources is supported by changes in ^{14}C activity of the bulk OC. Following the A.D. 1717 earthquake, the F_{mod} values range from 0.889 to 0.953 (Supplementary Table S1). Based on the SHCal13 calibration curve[36] constraint on the ^{14}C activity of atmospheric CO_2 and $OC_{biosphere}$ produced during this same period (i.e. between A.D. 1717 and A.D. 1795, Supplementary Table S2), the F_{mod} values of $OC_{biosphere}$ should be between 0.971 and 0.977. We normalise the F_{mod} values of organic matter in the lake to those of the atmosphere at time of deposition (Methods), and normalise the modern soil samples to the atmosphere at time of sampling[37], to better compare the measurements (Fig. 3B, Methods). The approach suggests the input of both surface and deeper soils immediately following the A.D. 1717 earthquake are required to produce the observed ^{14}C-depletion, supporting the observations from N/C and $\delta^{13}C$ (Fig. 3A).

Landslides are an effective mechanism of eroding and mixing deep and surface soils[4,32,38] and the geochemical data demonstrate these inputs are enhanced following the last four Alpine Fault earthquakes (Fig. 3). This is consistent with measurements made after the 2008 Wenchuan earthquake, which showed dilution of detrital ^{10}Be concentrations of quartz in river sediments due to an increase in the overall depth of erosion by landsliding[39]. Because the soil litters have a much higher organic carbon content (mean [TOC] = 12 ± 6 %, $n = 7$) compared to the deeper soils (mean [TOC] = 1.3 ± 0.8 %, $n = 6$), the composition of the lake sediments requires a large mass contribution from deeper soils to shift the composition (Fig. 3). With more measurements of the stock and composition of soil OC with depth, it may be possible to use organic matter to quantify the overall depth of landslide erosion[38] and how it evolves following a large earthquake[39]. At this stage, however, it is not possible to go beyond a qualitative analysis.

The large post-seismic increase in mountain-derived $OC_{biosphere}$ suggests that the river is not at transport capacity during the inter-seismic phases and can carry more $OC_{biosphere}$ than is supplied during those periods. This is consistent with the supply-limited nature of $OC_{biosphere}$ in other mountain rivers[11]. The post-seismic turbidite sequences suggest repeated hyperpycnal inputs to the lake in turbid river plumes[15,20] which effectively transport and preserve $OC_{biosphere}$, likely driven by high runoff intensities during storms[7,8,11]. Following the immediate response, each earthquake cycle shows a remarkably consistent evolution of $\delta^{13}C$ and C/N values (Fig. 2). The $OC_{biosphere}$ composition evolves away from that of deeper and higher elevation mountain soils and toward that of surface soils at lower elevations (Fig. 3A). ^{14}C-depleted organic matter appears to persist throughout the post-seismic phase (Fig. 3B). Landslide-derived material appears to be gradually removed from the catchment until the river reverts back to its inter-seismic state, perhaps due to a time lag associated with more poorly connected landslide deposits[7,14]. The time scale of this evacuation has been estimated from sediment core chronologies[20,29] to be 58 ± 15 years. Stabilisation of landslide scars by new vegetation growth may also play a role[40] and takes ~50–100 years in the Southern Alps[41].

Erosion and accumulation of organic carbon

To estimate the role of earthquakes in the accumulation of $OC_{biosphere}$ in the lake, we combined the measured [TOC] and the fraction of rock-derived OC in the core, with previously-determined clastic sedimentation rates[20] (Methods). This is a conservative measure because we do not account for $OC_{biosphere}$ stored in the co-seismic megaturbidites, which are likely to store some earthquake-derived landslide material[20]. The $OC_{biosphere}$ accumulation rate during the four post-seismic periods, as an uncertainty weighted-average over the core cross sectional area (Methods), was 11.8 ± 2.5 mg C cm^{-2} yr^{-1}, ranging from 9.8 ± 3.6 mg C cm^{-2} yr^{-1} to 15.6 ± 8.6 mg C cm^{-2} yr^{-1} (Table 1). This is 3.0 ± 0.7 times greater than the average $OC_{biosphere}$ accumulation rate for the inter-seismic periods of 3.9 ± 0.4 mg C cm^{-2} yr^{-1}. We find that four large earthquakes have driven the accumulation of 43 ± 5% of the $OC_{biosphere}$ deposited in the core from Lake Paringa since A.D. 965–887. Given an average post-seismic sedimentation phase duration of 58 ± 15 years[20,29], this period of deposition accounts for 23 ± 5% of the total record length (Supplementary Table S3).

The important role of earthquakes in the export of $OC_{biosphere}$ to Lake Paringa is consistent with wider estimates from the western Southern Alps. Based on inventories of landslides from large earthquakes[16-18,42,43], a $M_w \sim 8$ earthquake on the Alpine Fault would trigger extensive landslides in the temperate rainforest along the fault rupture. To estimate how much $OC_{biosphere}$ may be mobilized, we use an approach which describes landslide probability with distance from the epicenter accounting for seismic wave attenuation[42]. Based on a feasible range of peak landslide density after an Alpine Fault earthquake of 6-10 % of the land surface[13,17,18,42,43], and information on soil and vegetation carbon stocks[4,32], we estimate the total $OC_{biosphere}$ mass removed by an Alpine Fault earthquake as between 8 ± 4 Mt C and 14 ± 5 Mt C (Methods, Supplementary Fig. S2). Considering the recurrence interval of large earthquakes[30], the corresponding rate of $OC_{biosphere}$ erosion is between 5 ± 2 to 9 ± 4 t C km^{-2} yr^{-1}. These values are 70-100% of modern-day estimates of landslide-driven $OC_{biosphere}$ erosion[4] (~8 t C km^{-2} yr^{-1}) and 10-20% of modern-day estimates of total $OC_{biosphere}$ discharge by rivers (~39 t C km^{-2} yr^{-1}) in the western Southern Alps[32]. For context, the total mass which may be mobilized by an Alpine fault earthquake is potentially equivalent to New Zealand's annual CO_2 emissions of 9.439 Mt C in 2013 (ref. 44).

Implications for the geochemical carbon cycle

Seismogenic faults at convergent plate boundaries can impact carbon export from the terrestrial biosphere. Firstly, over million year timescales orogensis and denudation processes interact to build steep mountains[21,23]. These topographic barriers can intercept moisture[24] and fuel forest growth[25]. Such vegetated, steep landscapes promote $OC_{biosphere}$ erosion by runoff-driven processes and mass wasting[11] and mountain rivers can have very high $OC_{biosphere}$ yields[10]. As a result, it is estimated that ~40% of the global $OC_{biosphere}$ export by rivers may come from topography steeper than ~10° (3-arc-second)[11], which makes up ~16 % of Earth's continental surface[45]. A second impact to the carbon cycle occurs over decadal timescales, as demonstrated here, when the ground shaking during M_w > 7 earthquakes triggers widespread landsliding[16-18,42]. These landslides can deliver $OC_{biosphere}$ to rivers[19] which have the capacity to transport it (Fig. 3) and therefore result in pulsed increases in the organic carbon export from a mountain range (Fig. 2, Table 1). In the western Southern Alps, large earthquakes appear to have driven 43 ± 5 % of the $OC_{biosphere}$ export over the last thousand years. A single Alpine Fault earthquake could mobilize up to 14 ± 5 Mt C, ~10% of the estimated global annual $OC_{biosphere}$ discharge by rivers[10].

The links between tectonics and the carbon cycle are further pronounced when the fate of the eroded $OC_{biosphere}$ is also considered. Earthquake-triggered landslides act to greatly enhance clastic sediment yields in rivers in the years which follow the event[13-15]. This increases their turbidity and should act to increase sediment accumulation in depositional settings and increase the burial efficiency of $OC_{biosphere}$ and thus long-term CO_2 sequestration[8,10,12]. However, the role of terrestrial OC in the tectonic forcing of the carbon cycle is often neglected (in comparison to marine organic carbon burial[46]) partly because the global flux of $OC_{biosphere}$ erosion by earthquake-triggered landslides remains to be quantified. The widespread intersection of mountain forests and seismogenic faults, particularly in Oceania[47], could mean that active tectonics acts to moderate the drawdown of atmospheric CO_2 by $OC_{biosphere}$ burial and thus influence the long-term evolution of Earth's climate.

References

1. Garwood, N. C., Janos, D. P. & Brokaw, N. Earthquake-caused landslides: a major disturbance to tropical forests. *Science* **205,** 997-999 (1979).
2. Allen, R. B., Bellingham, P. J. & Wiser, S. K. Immediate Damage by an Earthquake to a Temperate Montane Forest. *Ecology* **80**, 708-714 (1999).
3. Veblen, T. T., & Ashton, D. H. Catastrophic influences on the vegetation of the Valdivian Andes, Chile. *Vegetatio* **36**, 149-167 (1978).

4. Hilton, R. G., Meunier, P., Hovius, N., Bellingham, P. J. & Galy, A. Landslide impact on organic carbon cycling in a temperate montane forest. *Earth Surf. Proc. Land.* **36**, 1670-1679 (2011).
5. Chen, H., Wu, N., Yuan, X., Gao, Y. & Zhu, D. Aftermath of the Wenchuan Earthquake. *Front Ecol. Environ.* 7**,** 72 (2009).
6. Hovius, N., Stark, C. P., & Allen, P. A. Sediment flux from a mountain belt derived by landslide mapping. *Geology* **25**, 231–234.
7. Rathburn, S. L. *et al*. The fate of sediment, wood, and organic carbon eroded during an extreme flood, Colorado Front Range, USA. *Geology* **45**, 499-502 (2017).
8. Kao, S. J. *et al.* Preservation of terrestrial organic carbon in marine sediments offshore Taiwan: mountain building and atmospheric carbon dioxide sequestration. *Earth Surf. Dyn.* **2**, 127-139 (2014).
9. Leithold, E. L. *et al.* Signals of watershed change preserved in organic carbon buried on the continental margin seaward of the Waipaoa River, New Zealand. *Marine Geology* **346**, 355–365 (2013).
10. Galy, V., Peucker-Ehrenbrink, B., & Eglinton, T. Global carbon export from the terrestrial biosphere controlled by erosion. *Nature* **521,** 204-207 (2015).
11. Hilton, R. G. Climate regulates the erosional carbon export from the terrestrial biosphere. *Geomorphology* **277**, 118-132 (2017).
12. Blair, N. E., & Aller, R. C. The fate of terrestrial organic carbon in the marine environment. *Ann. Rev. Mar. Sci.* **4,** 401-423 (2012).
13. Hovius, N. *et al.* Prolonged seismically induced erosion and the mass balance of a large earthquake. *Earth Planet. Sci. Lett.* **304,** 347-355 (2011).
14. Wang, J. *et al.* Controls on fluvial evacuation of sediment from earthquake-triggered landslides. *Geology* **43,** 115-118 (2015).
15. Dadson, S. J. *et al.* Earthquake-triggered increase in sediment delivery from an active

mountain belt. *Geology* **32,** 733-736 (2004).

16. Keefer, D. K. The importance of earthquake-induced landslides to long-term slope erosion and slope-failure hazards in seismically active regions. *Geomorphology* **10**, 265-284 (1994).
17. Li, G. *et al.* Seismic mountain building: Landslides associated with the 2008 Wenchuan earthquake in the context of a generalized model for earthquake volume balance. *Geochem. Geophy. Geosy.* **15,** 833-844 (2014).
18. Marc, O., Hovius, N., Meunier, P., Gorum, T., & Uchida T. A seismologically consistent expression for the total area and volume of earthquake-triggered landsliding. *J. Geophys. Res. Earth Surf.* **121**, doi:10.1002/2015JF003732 (2016).
19. Wang, J. *et al*. Earthquake-triggered increase in biospheric carbon export from a mountain belt. *Geology* **44**, 471-474 (2016).
20. Howarth, J. D., Fitzsimons, S.J., Norris, R.J. & Jacobsen, G. E. Lake sediments record cycles of sediment flux driven by large earthquakes on the Alpine fault, New Zealand. *Geology* **40,** 1091-1094 (2012).
21. Hovius N., Stark C. P., & Allen, P. A. Sediment flux from a mountain belt derived by landslide mapping. *Geology* **25**, 231–234 (1997).
22. Korup, O., McSaveney, M. J., & Davies, T. R. H. Sediment generation and delivery from large historic landslides in the Southern Alps, New Zealand. *Geomorphology* **61**, 189-207 (2004).
23. Norris, R. J., & Cooper, A. F. Late Quaternary slip rates and slip partitioning on the Alpine Fault, New Zealand. *Journal of Structural Geology* **23**, 507–520 (2001).
24. Henderson, R. D., & Thompson, S. M. Extreme rainfalls in the Southern Alps of New Zealand. *Journal of Hydrology (New Zealand)* **38**, 309–330 (1999).
25. Bellingham, P. J., & Richardson, S. J. Tree seedling growth and survival over 6 years across different microsites in a temperate rain forest. *Canadian Journal of Forest Research* **36**, 910–918 (2006).

26. Sutherland, R., *et al.* Do great earthquakes occur on the Alpine Fault in central South Island, New Zealand? in Okaya, D., et al., eds., A continental plate boundary: Tectonics at South Island, New Zealand: American Geophysical Union Geophysical Monograph 175, p. 235–251 (2007).
27. Wells, A., Yetton, M.D., Duncan, R.P., & Stewart, G.H. Prehistoric dates of the most recent Alpine fault earthquakes, New Zealand. *Geology* **27**, 995–998 (1999).
28. Berryman, K. R. et al. Late Holocene rupture history of the Alpine Fault in South Westland, New Zealand. *Bull. Seismol. Soc. Am.***102**, 620–638 (2012).
29. Howarth, J. D., Fitzsimons, S. J., Norris, R. J., & Jacobsen, G.E. Lake sediments record high intensity shaking that provides insight into the location and rupture length of large earthquakes on the Alpine Fault, New Zealand. *Earth Planet. Sci. Lett.* **403**, 340–351 (2014).
30. Howarth, J. D., Fitzsimons, S. J., Norris, R. J., Langridge, R., & Vandergoes, M. J. A 2000 yr rupture history for the Alpine Fault derived from Lake Ellery, South Island, New Zealand. *Geol. Soc. Am. Bull.***128**, 627–643 (2015).
31. Cochran U. A. *et al.* A plate boundary earthquake record from a wetland adjacent to the Alpine fault in New Zealand refines hazard estimates. *Earth Planet. Sci. Lett.* **464,** 175–188 (2017)
32. Hilton, R. G., Galy, A., & Hovius, N. Riverine particulate organic carbon from an active mountain belt: Importance of landslides. *Global Biogeochem. Cycles* **22**, GB1017, doi :10.1029/2006GB002905 (2008).
33. Nibourel, L., Herman, F., Cox, S. C., Beyssac, O., & Lavé, J. Provenance analysis using Raman spectroscopy of carbonaceous material: A case study in the Southern Alps of New Zealand. *J. Geophys. Res. Earth Surf.* **120**, 2056–2079 (2015).
34. Horan, K. *et al.* Mountain glaciation drives rapid oxidation of rock-bound organic carbon. *Sci. Adv.* **3**, e1701107, doi:10.1126/sciadv.1701107 (2017).

35. Ehleringer, J. R., Buchmann, N., & Flanagan, L. B. Carbon isotope ratios in belowground carbon cycle processes. *Ecological Applications* **10**(2), 412–422 (2000).

36. Hogg, A. G. *et al.* SHCal13 Southern Hemisphere calibration, 0–50,000 years cal BP. *Radiocarbon* **55**, 1889–1903 (2013).

37. Soulet, G., Skinner, L. C., Beaupré, S. R., & Galy, V. A Note on Reporting of Reservoir ^{14}C Disequilibria and Age Offsets. *Radiocarbon* **58**, 205-211 (2016).

38. Larsen, I. J., Montgomery, D. R. & Korup, O. Landslide erosion caused by hillslope material. *Nature Geoscience* **3**, 247-251 (2010).

39. West, A. J. *et al.* Dilution of ^{10}Be in detrital quartz by earthquake-induced landslides: Implications for determining denudation rates and potential to provide insights into landslide sediment dynamics. *Earth Planet. Sci. Lett.* **396,** 143-153 (2014).

40. Restrepo, C. *et al.* Landsliding and its multiscale influence on mountainscapes. *Bioscience* **59,** 685-698 (2009).

41. Coomes, D. A., Holdaway, R. J., Kobe, R. K., Lines, E. R., & Allen, R. B. A general integrative framework for modelling woody biomass production and carbon sequestration rates in forests. *Journal of Ecology* **100**, 42–64 (2012).

42. Meunier, P., Hovius, N., & Haines, A.J. Regional patterns of earthquake-triggered landslides and their relation to ground motion. *Geophys. Res. Lett.* **34**, L20408, doi:10.1029/2007GL031337 (2007).

43. Roback, K., *et al.* The size, distribution, and mobility of landslides caused by the 2015 Mw7.8 Gorkha earthquake, Nepal. *Geomorphology* 301, 121-138 (2017).

44. New Zealand's Greenhouse Gas Inventory 1990–2013, http://www.mfe.govt.nz/publications/climate-change/new-zealands-greenhouse-gas-inventory-1990-2013

45. Larsen, I. J., Montgomery, D. R., & Greenberg, H. M. The contribution of mountains to global denudation. *Geology* **42**, 527–530 (2014).

46. Shields, G. A. & Mills, B. J. W. Tectonic controls on the long-term carbon isotope mass balance. *Proceedings of the National Academy of Sciences* 114, 4318-4323 (2017).
47. Kreemer, C., Holt, W. E., & Haines A. J. An integrated global model of present-day plate motions and plate boundary deformation. *Geophysical Journal International* **154**, 8–34 (2003).

Acknowledgements

N.V.F. completed the research as part of the MSci programme in Geography at Durham University. We thank Hugo Bloor and Adelaine Moody for field support and Dr Eleanor Maddison, Kathryn Melvin, Alison George, Martin West and Amanda Hayton for laboratory support. Samples were collected under Department of Conservation research license (39411-GEO). Funding was provided by a Durham University Seedcorn Grant, a Natural Environment Research Council (NERC), UK, Standard Grant to R.G.H., A.L.D., E.L.M. and J.D.H. (NE/P013538/1), a Rutherford Foundation Postdoctoral Fellowship to J.D.H. (RFTGNS1201-PD) and COFUND Junior Research Fellowship at Durham University to J.W.

Author contributions

R.G.H., J.D.H. and A.L.D. conceived and designed the project. J.D.H. and S.J.F. collected the core and N.V.F. undertook the sampling and geochemical analysis under the supervision of R.G.H., J.D.H. and D.G. J.W. undertook the biomarker analysis and interpretation under direction from E.L.M. and R.G.H. J.D. ran the radiocarbon analyses. N.V.F. analysed and interpreted the bulk data under the supervision of R.G.H., A.L.D. and J.D.H. T.C. computed the Alpine Fault landslide scenarios with R.G.H. and J.D.H. R.G.H., N.V.F., and J.D.H. wrote the paper with input from all authors.

Competing Financial Interests statement

The authors declare they have no competing financial interests.

Additional information

Supplementary information is available for this paper

Reprints and permissions information is available at www.nature.com/reprints.

Correspondence and requests for materials should be addressed to R.G.H. r.g.hilton@durham.ac.uk

Figure Captions

Figure 1: Tectonic setting of the Southern Alps and the topography of the Lake Paringa catchment. A. Regional tectonic setting. **B**. The source catchment of Lake Paringa (outlined in yellow) and the location of sediment core PA6m1. Dots show location of other cores[20]. **C**. Comparison of the topography of the Windbag Basin catchment (yellow) and the adjacent Paringa River (blue), a major trunk valley on the western flank of the Southern Alps derived from an 8 m Digital Elevation Model. **D.** Hillslope angle probability density functions showing that the Windbag Basin (yellow) is comparable to neighboring Paringa catchment (blue).

Figure 2: Organic matter in Lake Paringa core PA6m1. Left to right, core images, graphic log, dry mass of clastic sediment (Mcs, g) and magnetic susceptibility (X) for **A.** core PA1 (ref. 20) and **B**. PA6m1 (this study), which correlate at the centimeter scale (black – 5 cm running average; grey– 0.5 cm resolution data). For PA6m1, the stable isotope composition of organic carbon ($\delta^{13}C$, ‰ analytical uncertainty smaller than the symbol size) and the organic carbon to nitrogen ratio (C/N,

colours). Four large Alpine Fault earthquakes are recorded by megaturbidites (grey bars)[20] and post-seismic periods are highlighed by pink bars.

Figure 3: Sources of organic matter in Lake Paringa during earthquake cycles. Symbols denote post-seismic sediments after each major earthquake identified in the core[20] and are coloured by sample distance (in cm) above the megaturbidite marking the previous earthquake (yellow are immediately post-seismic). Stars and hexagons show soil and weathered colluvium samples (Supplementary Table S2). Analytical uncertainties are smaller or similar to the symbol size. **A.** The nitrogen to organic carbon ratio versus the stable C isotope composition. **B.** The radiocarbon disequilibria of samples, $F^{14}R_{x\text{-}atm}$, relative to the atmosphere[37] (Methods), allowing comparison between lake sediment samples deposited post-A.D. 1717 and modern-day soils.

Methods

Study site and Core collection

The western Southern Alps are an ideal location to track $OC_{biosphere}$ erosion due to the repeated large earthquakes[20], rapid erosion[21,22], and extensive vegetation cover[25]. The maritime climate results in high rates of orographic precipitation of up to 10-12 m yr^{-1} (ref. 24). The tectonic and climatic setting drive physical erosion rates of 6-9 mm yr^{-1} adjacent to the Alpine fault, where modal slope angles of ~35° promote bedrock landslides which supply sediment to rivers during the current inter-seismic period[4,21,22]. Temperate rainforest is found at elevations ≤ 800 m[25,48]. At altitudes below 400 m, evergreen angiosperms, conifers, *Dacrydium cupressinum*, and *Dacrycarpus dacrydioides* preside, while shrubs, herbs and grassland persist above the regional snowline at ~1,250 m. The carbon stocks of above-ground biomass and soil in the western Southern Alps are estimated to be 17,500 ± 5,500 tC km^{-2} and ~18,000 ± 9,000 tC km^{-2}, respectively[4]. In the current inter-seismic phase, steep slopes and high precipitation result in high particulate $OC_{biosphere}$ fluxes by rivers[32,49], with the mean of ~39 tC km^{-2} yr^{-1} being amongst the highest in the world[10,11].

The catchment above Lake Paringa drains approximately 60 km^2 of the frontal Southern Alps with elevations from 16-1420 m (Fig. 1A). Median hillslope gradients of ~31-32° are sufficient to support high rates of landsliding[21,22] and are similar to those in other larger catchments in the western Southern Alps (Fig. 1D). Four soil samples were recovered from a 0.99 m deep soil pit at 75 m elevation close to Lake Paringa (Supplementary Table S2). Together these represent the O- (surface), A- (0.01-0.09 m), E- (0.09-0.79) and B- (>0.79 m) soil horizons. Three proximal surface soil samples were collected from low elevation (15 m) on the Lake Paringa fan. Catchment soils[34] (litters and weathered colluvium samples) come from a published[34] elevation transect (420 – 750 m) collected from Alex Knob in another watershed ~70 km northeast of the study area along strike of the Alpine Fault (Supplementary Table S2). This site is analogous to the Lake Paringa headwaters because the vegetation cover is similar[48], both are located at the mountain front within a few km of the Alpine Fault, and have the same range in elevation (400-800 m), mean annual precipitation[50], slope angles (30-50 degrees), and bedrock geology[51].

The 6 m sediment core was collected from the center of the Windbag Basin, Lake Paringa, using a Mackereth corer (PA6m1) (Fig. 1B). The core was correlated to master core PA1 (Fig. 2) which has a well-established chronology[20] based on accelerator mass spectrometry measurements of the radiocarbon (^{14}C) content of 22 terrestrial macrofossils. Howarth et al. (2012) (ref. 20) derived a calibrated calendar age for each macrofossil in OxCal 4.1 using the P_sequence depositional model. Stratigraphic horizons of the master core were visually correlated to coincident horizons on the recovered core (Fig. 2A&B). Where visual correlation was not possible, the extracted core was correlated to the master core using a linear regression model. As the downcore correlation resolution of ≥ 0.1 cm is greater than the sediment sampling resolution of ≥ 0.5 cm, minor correlation errors are assumed to be negligible.

Geochemical Analyses

A total of 189 samples were collected from core PA6m1 at variable intervals of 0.2–5.8 cm (Table S1). For each of these samples, along with the soil samples, 0.4–0.6 g was reacted with 20 ml of 0.25 M hydrochloric acid for four hours at approximately 70°C to remove any inorganic carbonate present in the sample material. Reaction conditions were determined following tests on material collected from the nearby Poerua and Whataroa catchments to maximize the preservation of organic material while effectively removing detrital carbonates derived from the catchment[52]. Total organic carbon content ([TOC], wt. %) and stable organic carbon isotopes ($\delta^{13}C$, ‰) were measured by combustion of sediment at 1020°C in a Costech Elemental Analyser coupled via a CONFLO III to a MAT 253 stable isotope mass spectrometer. [TOC] measurements were corrected for mass loss during reaction. $\delta^{13}C$ measurements were normalised based on a range of internal and international standards and corrected for instrumental blanks. Total nitrogen content ([TN], %) was measured by combustion of untreated samples in a Costech Elemental Analyser with a CARBOSORB trap to inhibit large CO_2 peaks from affecting measurements. Sample replicates (n = 20) were used to determine precisions (±2SE) of [TOC] = ±0.12%, $\delta^{13}C$ = ±0.11‰ and [TN] = ±0.01%. These are assumed to account for heterogeneity within the dataset.

A subset of samples were selected from two of the seismic cycles in the lake sediments (cycles 4 and 5, Table 1) across inter-seismic (n = 4), post seismic (n = 8) and co-seismic (n = 3) sediments for the analysis of biomarker abundance following published methods[53,54] (Supplementary Table S4). We focused on the extraction of *n*-alkanes and *n*-alkanoic acids from aliquots of lake sediment (~2g) to which internal standards were added prior to extraction in a microwave accelerated reaction system (MARS, CEM Corporation) in 12 mL of dichloromethane (DCM) and methanol (3:1). Total lipid extracts were saponified at 70 ºC for 1 h using 8% KOH in methanol/water (99:1). The 'base' fractions were liquid–liquid extracted in 2.5 mL of pure hexane three times. The 'acid' fractions were extracted at pH 2 with 2.5 mL hexane and DCM (4:1) three times. Alkanoic acids in the acid fraction were methylated in 3 ml mixture of HCl and methanol (5:95) at 70 ºC for 12 h. MilliQ water (4 mL) was then added, and fatty acid methyl esters (FAMEs) were liquid–liquid extracted into hexane and DCM (4:1) three times. The base fractions were separated into three sub-fractions by silica column chromatography, eluting with: 4 mL hexane (F1); 4ml DCM (F2) and 4ml MeOH (F3). The *n*-alkanes in the first fraction of the base fraction and the FAMEs were quantified using a gas chromatograph (GC) fitted with a flame ionization detector (FID; Thermo Scientific Trace 1310). Hydrogen was used as a carrier gas. The temperature increased from 70°C (initial hold time 2 min) to 170°C at a rate of 12°C min^{-1} then to 310 °C at 6°C min^{-1} and held for 35 min. Quantification was achieved by comparison with internal standard Hexatriacontane and Heptadecanoic acid (Sigma-Aldrich). All measurements were made at the Department of Geography, Durham University.

Samples (n = 23) from the A.D. 1717 seismic event sequence were selected and analysed for the radiocarbon activity (^{14}C, reported as 'fraction modern', F_{mod}) of bulk organic matter by accelerator mass spectrometry after graphitization at the Rafter Radiocarbon Laboratory, New Zealand (Supplementary Table 1). IAEA-C5, an international standard, was subjected to the same inorganic carbonate removal process and measured for F_{mod}. This returned F_{mod} within 0.0125 of expected values. Published measurements of F_{mod} from soils[34] are compiled here (Supplementary Table 2).

To compare the ^{14}C activity of lake core sediment samples from after the A.D. 1717 earthquake to those of modern soils (Fig. 3B), we calculated the ^{14}C disequilibria relative to the atmosphere[37], $F^{14}R_{x\text{-}atm}$:

$$F^{14}R_{x-atm} = \frac{Fmod-x}{Fmod-atm} \qquad \text{(equation 1)}$$

where $F_{mod\text{-}x}$ is the fraction modern of the sample, and $F_{mod\text{-}atm}$ is that of the atmosphere at the time of sampling (for modern samples) or deposition (for sediment samples). $F^{14}R_{x\text{-}atm}$ contains information on the residence time of carbon in a reservoir, although this is not a linear function with sample age[37]. Here it provides a useful way to compare the ^{14}C activity of organic matter in the lake core to the modern day soil samples.

For the soil samples[34], we used $F_{mod\text{-}atm} = 1.0354$ based on atmospheric CO_2 measurements at Wellington, New Zealand[55] and the sampling date of October 2014. The two soil litter samples (NZ14-57 and NZ14-60, Supplementary Table S2) contain bomb-derived ^{14}C, and so are not fully analogous to the composition of soil present in the pre-anthropogenically disturbed environment of New Zealand. For the lake sediment samples, the chronology is well constrained[20], but the details of post-seismic sedimentation rates are not known. For that reason, we normalized all lake sediment F_{mod} values to a single $F_{mod\text{-}atm}$ value of between 0.9712 and 0.9809 (i.e., the mid-value and range of $F_{mod\text{-}atm} = 0.9760 \pm 0.0049$), which represents values for A.D. 1715 to A.D. 1795 (the approximate duration of the post-seismic phase) from ShCal13[36].

Organic carbon source and OC accumulation rates

The total mass deposited during each seismic phase was determined for PA6m1, following the correlation to the master core PA1[20]. Uncertainties on total mass accumulation were quantified by a Monte Carlo simulation, taking into account the uncertainties on the correlation and the uncertainties on the age model and duration of each interval (Supplementary Table S3). To quantify the OC accumulation rate, the average [TOC] value for each of the post-seismic and inter-seismic phases were combined with the total mass accumulation rate. Whilst this is not a volumetric estimate, it does quantify millennial-scale changes in the relative rates of OC supply. We omitted the post-seismic phase following the ca. A.D. 1570 seismic event[20] (referred to as 'Seismic phase 2' in previous work), because the Alpine Fault did not rupture as far south as Lake Paringa, if at all[20,26,29,30], thus it is not comparable with the other events. In addition, this method does not account for OC deposited in co-seismic megaturbidites. These are predominantly composed of re-worked sub-aqueous material, but may contain sediment from slope failures immediately adjacent to the margins of Lake Paringa, and so the role of earthquakes may be underestimated.

To report $OC_{biosphere}$ accumulation, rock-derived OC inputs to Lake Paringa are accounted for. The fraction of rock-derived, 'petrogenic', organic carbon, F_{petro}, can be quantified[10,11] using measured [TOC] and a previously-defined bedrock end-member for the region[32-34], an average [TOC] ~ 0.15%, and assuming a binary mixture of rock OC and biospheric OC[10,32]. This returns mean F_{petro} values for each depositional phase which are < 0.1 and does not systematically vary between inter-seismic and post-seismic phases (Supplementary Table S3). The $OC_{biosphere}$ accumulation rates were then calculated by combining OC accumulation rate and the fraction of carbon from biospheric sources (i.e. 1 - F_{petro}). Uncertainties derive from the proportion of uncertainties on total mass accumulation rate (described above) and the 2 x standard error of the mean [TOC] and F_{petro} values for each depositional phase (Supplemental Table S3).

To compare the rates of $OC_{biosphere}$ accumulation (mgC cm^{-2} yr^{-1}) between inter-seismic and post-seismic phases, we calculate the uncertainty-weighted average of all events (Table 1). This views each post-seismic (and inter-seismic) phase as measurements of the same quantity and accounts for the associated uncertainty (i.e. the fact that some of the measurements are more precise than others). Based on these values, the $OC_{biosphere}$ accumulation rates are 3.0 ± 0.7 times faster than inter-seismic rates. The arithmetic mean is more appropriate if each post-seismic (and inter-seismic) phase are viewed as discrete entities (i.e. they are not replicate measurements of the same phenomenon) and gives a corresponding value of 2.4 ± 1.9. The comparison of uncertainty-weighted mean values (Table 1) is reported in the text based on the observed similarity of the geochemical responses to each large earthquake (Figs. 2, 3) and regularity of Alpine Fault rupture frequency and length based on palaoseismic evidence[28,30,31].

To determine the relative importance of large earthquakes in the total mass of $OC_{biosphere}$ accumulation, we sum all inter-seismic and post-seismic masses (mgC) and report the proportion of the total ($7.95 \times 10^4 + 5.94 \times 10^4 = 13.9 \times 10^4$ mgC) represented by $OC_{biosphere}$ during the post-seismic phases (5.94×10^4 mgC), which is 42.7 ± 5.4 %. The uncertainty is derived from the propagation of errors during addition of each seismic cycle.

Landslide-mobilized $OC_{biosphere}$ by an Alpine Fault earthquake

To estimate the likely magnitude of $OC_{biosphere}$ erosion by an Alpine Fault earthquake over the entire length of the fault rupture, and to enable a comparison of this to the values derived from the detailed Lake Paringa record, we used published literature and a theoretical framework to provide a bound on the main variables. The rupture length of the A.D. 1717 earthquake is estimated to be >380 km[31], and previous Alpine Fault earthquakes are thought to have ruptured between 250 km and 350 km based on palaeoseismic reconstructions[26,30]. We used a rupture length of 300 km as a conservative estimate. We examined the slope angles as a function of distance to the fault using 30 m resolution digital topographic data from SRTM[56] for a typical elevation profile from the nearby Whataroa catchment, and found that steep slopes capable of sustaining earthquake-triggered landslides (> 20°)[18,43] are present up to and beyond ~25 km of the Alpine Fault (Supplementary Fig. S2A). To constrain the area of landslides in mountain forest following a M_w ~8 Alpine Fault earthquake, we used a model accounting for seismic wave attenuation which has been tested on empirical data[42]:

$$P_{ls}(R) = \frac{aR_0 \exp\left(\frac{R_0}{\chi}\right)}{R} \exp\left(-\frac{R}{\chi}\right) \qquad \text{(equation 2)}$$

where $P_{ls}(R)$ is the percentage of surface area impacted by co-seismic landslides as a function of distance to the earthquake epicentre (R), a is a constant reflecting an seismogenic source term and the geomorphic sensitivity to ground motion, χ is a damping factor here set to 4 km, and R_0 is the focal depth[42], here set to 10 km (Supplementary Fig. S2B). The total landslide area is computed as:

$$A_{ls,tot} = L \int_{R_{min}}^{R_{max}} P_{ls}(R)\, dR \qquad \text{(equation 3)}$$

where L is the rupture length, here fixed at 300 km, R_{min} is the intersection of the Alpine Fault with the surface and R_{max} is the maximum distance from the fault where landsliding is more than ~0.2%. Here this equates to R_{max} = 20 km. Using the estimates of $OC_{biosphere}$ stocks in vegetation (OC_{veg} = 17500 ± 5500 tC km^{-2}) and soils (OC_{soil} = 18000 ± 9000 tC km^{-2}) (ref. 4), the total mass of organic carbon, m_{OC} tC km^{-2}, mobilized by a M_w = 8 earthquake is given by:

$$m_{OC} = (OC_{veg} + OC_{soil})A_{ls,tot} \qquad \text{(equation 4)}$$

The mobilization rate, tC km^{-2} yr^{-1}, is calculated assuming a M_w ~ 8 recurrence time of 263 ± 68 years[30]. The maximum value of P_{ls} is not known for an Alpine Fault earthquake, but it is reasonable to assume it may vary somewhere between 2.5% (M_w7.6 Chi Chi earthquake Taiwan[13,42]) to 12 % (M_w7.9 Wenchuan earthquake, China[17,57]). A range of scenarios between these values are considered (Supplementary Fig S2C). While these calculations remain untested for an Alpine Fault earthquake, they represent reasonable impacts based on our current understanding of earthquake-triggered landslides and available empirical data on landslide distributions. These estimates account for both vegetation and soil, with a wide range of grain sizes, meaning their subsequent mobilization and transport through river networks might be out of phase over annual to decadal timescales[7,11].

Data and Code Availability

The authors declare that the data supporting the findings of this study are available within the article and its Supplementary Information files and Supplementary Tables (S1-S4). We have opted not to make the computer code associated with the landslide modelling presented in this paper available because the governing equations are provided (Equations 2-4).

References only in Methods

48. Reif, A., & Allen, R. B. Plant communities of the steepland conifer–broadleaved hardwood forests of central Westland, South Island, New Zealand. *Phytocoenologia* **16**, 145–224 (1988).

49. Carey, A.E., *et al.* Organic carbon yields from small, mountainous rivers, New Zealand. *Geophysical Research Letters* **32**, L15404, doi:10.1029/2005GL023159 (2005).

50. Tait, A., Henderson, R., Turner, R, & Zheng, X. Thin plate smoothing spline interpolation of daily rainfall for New Zealand using a climatological rainfall surface. *Int. J. Climatol.* **26**: 2097–2115 (2006)

51. Cox, S. C., & Barrell, D. J. A. *Geology of the Aoraki Area,* Institute of Geological and Nuclear Science, 1:250,000 Geological Map 15, GNS Science, Lower Hutt (2007).

52. Galy, V., Bouchez, J., & France-Lanord, C. Determination of total organic carbon content and $\delta^{13}C$ in carbonate-rich detrital sediments. *Geostand. Geoanal. Res.* **31**, 199–207 (2007).

53. Hemingway, J. D. *et al.* Multiple plant-wax compounds record differential sources and ecosystem structure in large river catchments. *Geochim. Cosmochim. Acta*. **184**, 20-40 (2016).

54. Bachem, P. E., Risebrobakken, B., De Schepper, S., & McClymont, E. L. Highly variable Pliocene sea surface conditions in the Norwegian Sea. *Clim. Past.* **13**, 1153-1168 (2017).

55. Turnbull, J. C., *et al.* Sixty years of radiocarbon dioxide measurements at Wellington, New Zealand 1954–2014, *Atmos. Chem. Phys. Discuss*. https://doi.org/10.5194/acp-2016-1110 (2016).

56. Schwanghart, W., & Scherler, D. TopoToolbox 2 - MATLAB-based software for topographic analysis and modeling in Earth surface sciences. *Earth Surface Dynamics* **2**, 1-7 (2014).

57. Li, G. *et al.* Connectivity of earthquake-triggered landslides with the fluvial network: implications for landslide sediment transport after the 2008 Wenchuan earthquake. *Journal of Geophysical Research - Earth Surface* **121**, 703-724 (2016).

Table 1: Organic carbon accumulation rates in Lake Paringa core PA6m1.

Seismic cycle*	Date of Alpine Fault Rupture* (yrs A.D.)	95% age range for megaturbidite deposition* (yrs A.D.)	Post-seismic $OC_{biosphere}$ accumulation rate (mg C cm^{-2} yr^{-1})**	Inter-seismic $OC_{biosphere}$ accumulation rate (mg C cm^{-2} yr^{-1})**
1	1717	1745-1690	14.4 ± 5.2	9.6 ± 6.5
3	ca. 1400	1405-1374	15.6 ± 8.6	4.4 ± 0.6
4	ca. 1150	1120-1064	9.8 ± 3.6	3.5 ± 0.6
5	ca. 925	965-887	11.7 ± 5.3	3.7 ± 1.0
*All events****			*11.8 ± 2.5*	*3.9 ± 0.4*

*from ref. 20

**see Supplementary Table S3

***Uncertainty-weighted average

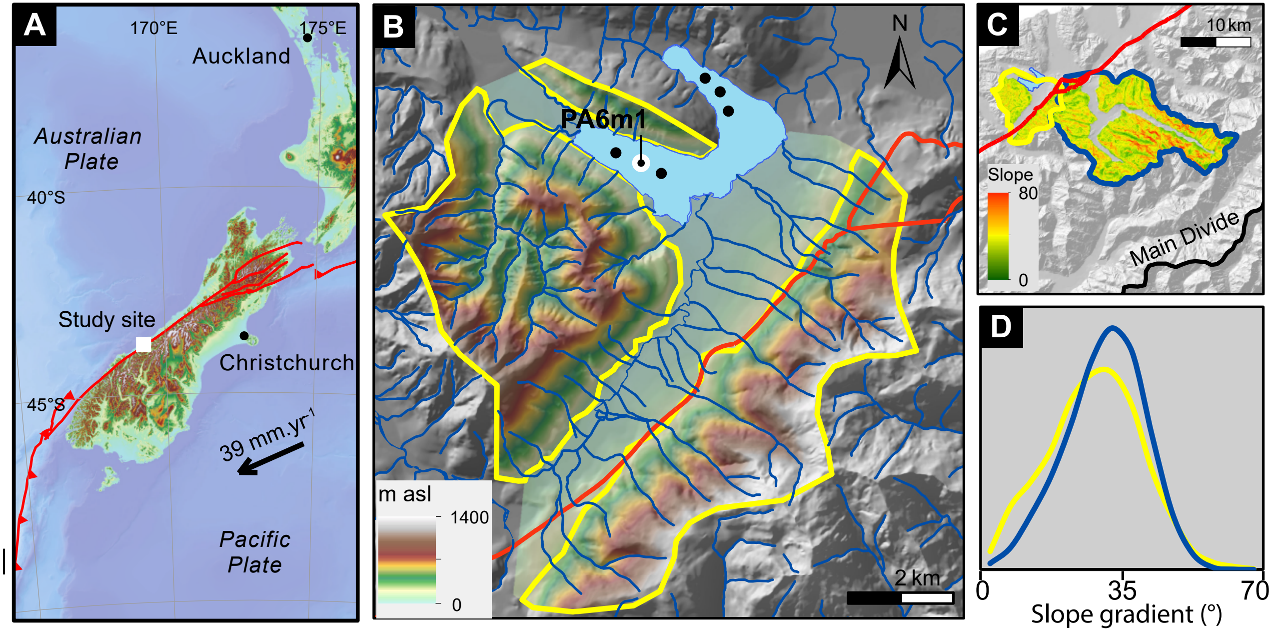

A
170°E
175°E
Auckland
Australian Plate
40°S
Study site
Christchurch
45°S
39 mm.yr-1
Pacific Plate
B
N
PA6m1
m asl
1400
0
2 km
C
10 km
Slope
80
0
Main Divide
D
0
35
70
Slope gradient (°)

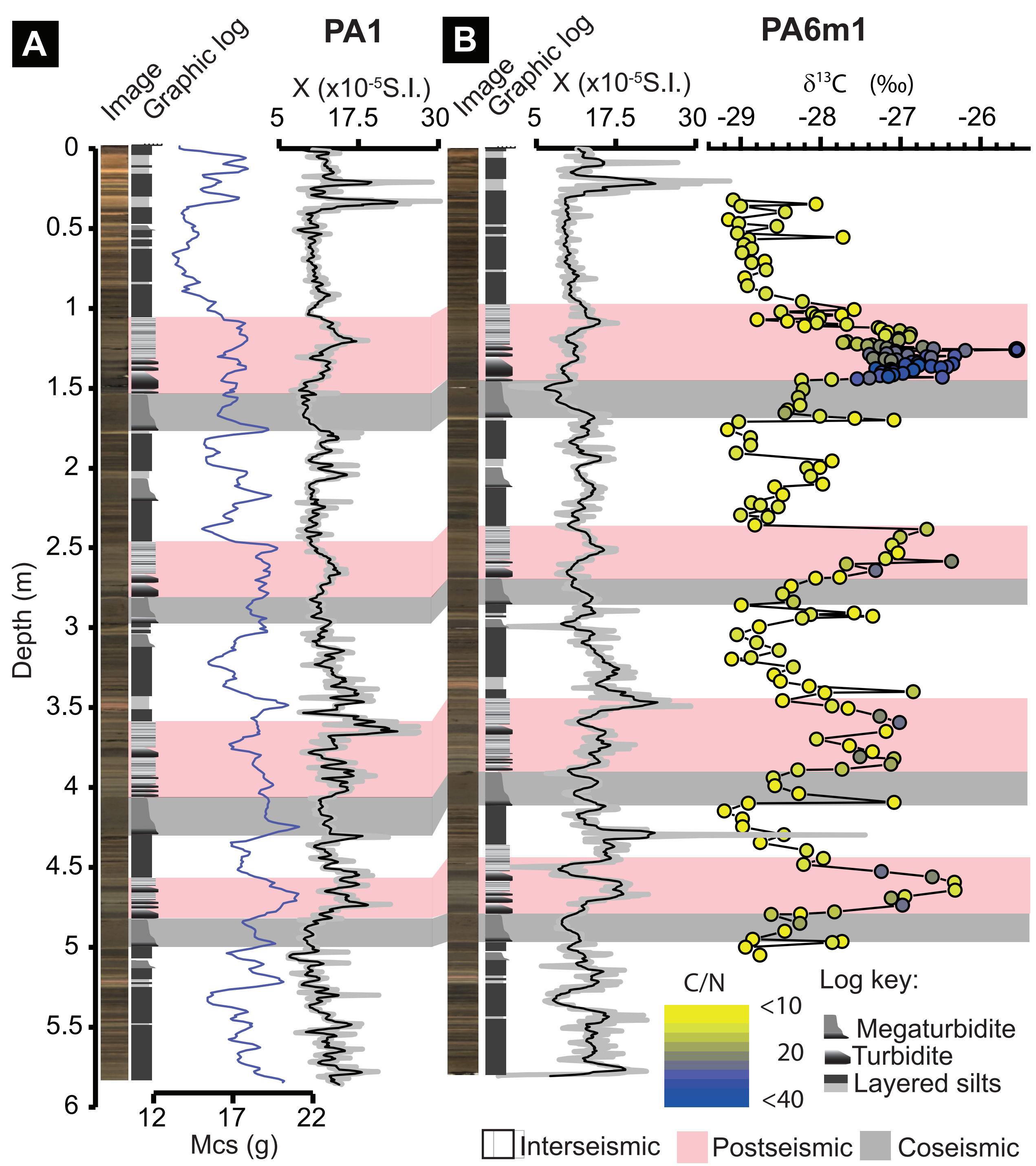

A
PA1
B
PA6m1
Image
Graphic log
X (x10-5S.I.)
5 17.5 30
δ13C (‰)
-29 -28 -27 -26
Depth (m)
Mcs (g)
12 17 22
C/N
<10
20
<40
Log key:
Megaturbidite
Turbidite
Layered silts
Interseismic
Postseismic
Coseismic

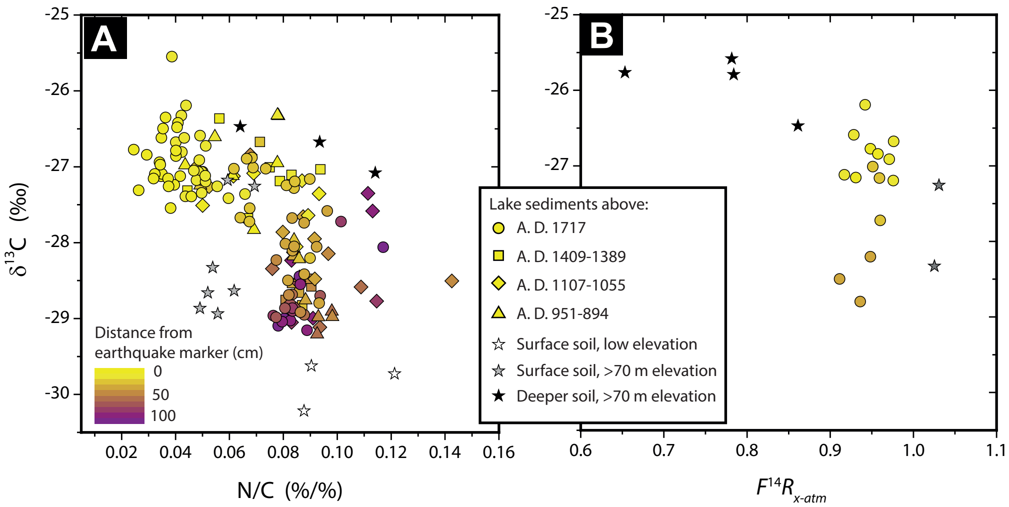

A
B
δ13C (‰)
N/C (%/%)
F14Rx-atm
Distance from earthquake marker (cm)
0
50
100
Lake sediments above:
A. D. 1717
A. D. 1409-1389
A. D. 1107-1055
A. D. 951-894
Surface soil, low elevation
Surface soil, >70 m elevation
Deeper soil, >70 m elevation